Chapter 1

Results

1.1 Correlation of Parameters

We observe correlation between two parameters using the statistical definition of the correlation coefficient ($\rho_{X,Y}$), defined in Eqn. **??**.

$$\rho_{X,Y} = \frac{cov(X,Y)}{\sigma_X \sigma_Y} \tag{1.1}$$

cov represents covariance, and σ represents the standard deviation of a set X. The correlation coefficient is unitless, and measured from -1.0 $< \rho_{X,Y} <$ 1.0. A correlation coefficient of 0 indicates the variables X and Y are uncorrelated, while -1.0 indicates the variables are perfectly inversely correlated; likewise, a correlation coefficient of 1.0 means X and Y are perfectly correlated. Correlation coefficient is used to estimate an environmental parameter's potential usefulness for calculating a new *coneR1* for use in an

Dataset	ρ_α
PETS1	0.199
PETS2	0.671
aton_highway1	0.684
aton_highway3	0.742
aton_room	0.548
aton_campus	0.360
aton_hallway	0.656
aton_lab	0.695

Table 1.1: Datasets and their α_{dB} correlations to *coneR1**.

arbitrary environment. We represent the correlation between *coneR1** and α as ρ_α.

1.1.1 *coneR1** and Average Attenuation

Both attenuation models (α_{dB} and $\alpha_{\%\Delta}$) were considered for correlation against the *coneR1** values of a dataset. Correlation ρ_α is represented for both attenuation models as ρ_{dB} and $\rho_{\%\Delta}$ respectively. Results for both are illustrated below in Figure **??** and Figure **??**. Tables **??** and **??** present correlation coefficients for each dataset for α_{dB} and $\alpha_{\%\Delta}$.

Both Tables **??** and **??** demonstrate significant correlation between *coneR1** and α, consistent across all datasets. For example reference, an arbitrary variable (number of normal SIFT features detected) has been correlated against *coneR1** (Table **??**). We observe positive and negative correlations, as well as strong and weak correlations. This illustrates the significance found in the consistent positive α correlations across datasets. Strong and consistent

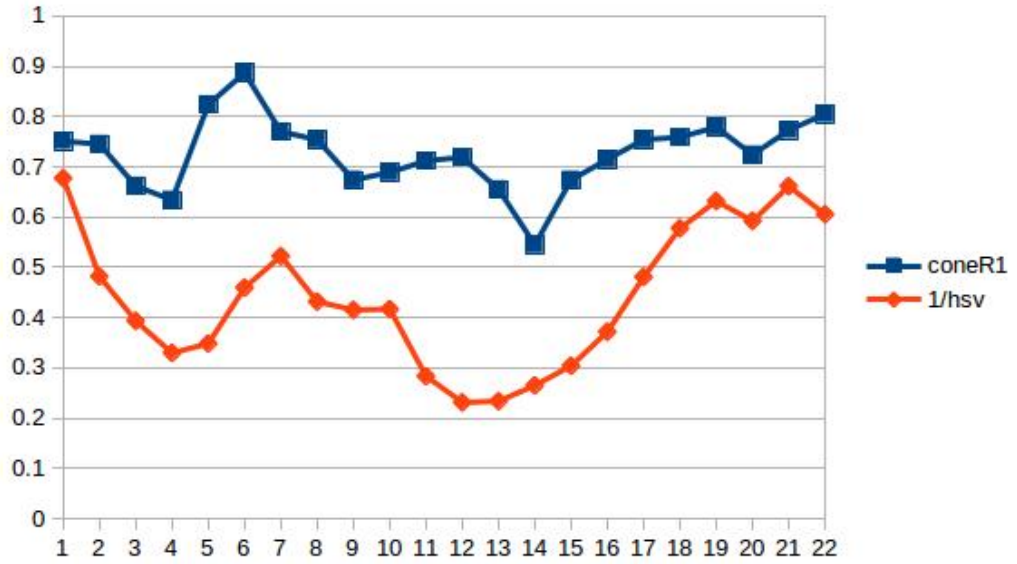

(a) aton_room

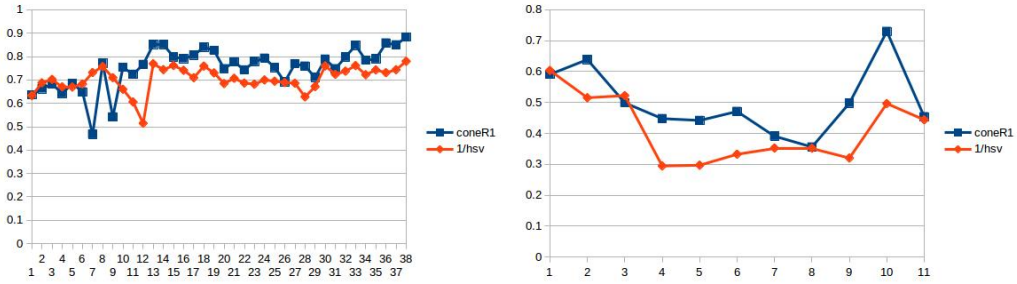

(b) aton_campus (c) PETS2

Figure 1.1: Visual correlation of α_{dB} (orange) and *coneR1** (blue) is observed, for a selection of datasets. (All results can be found in the appendix)

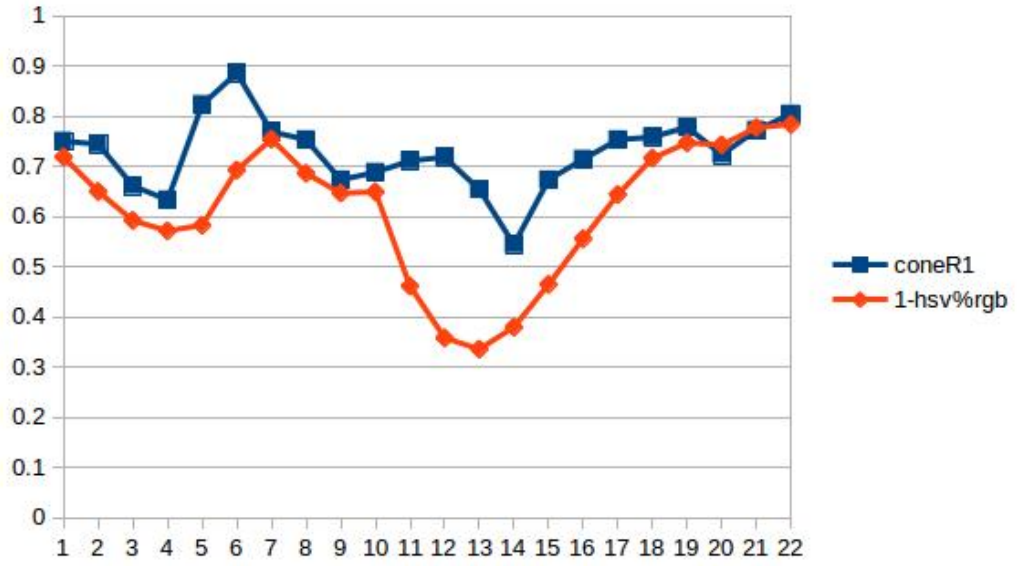

(a) aton_room

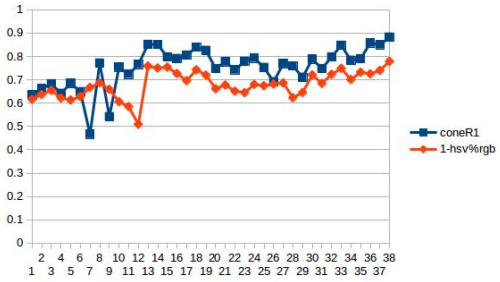

(b) aton_campus

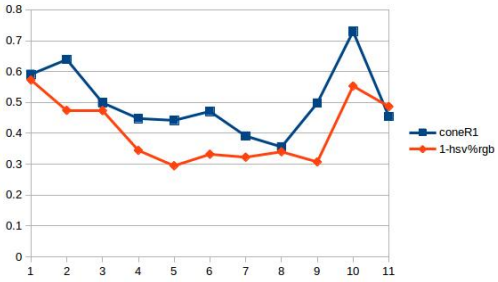

(c) PETS2

Figure 1.2: Visual correlation of $\alpha_{\%\Delta}$ (orange) and *coneR1** (blue) is observed, for a selection of datasets. (All results can be found in the appendix)

Dataset	$\rho_{\%\Delta}$
PETS1	0.184
PETS2	0.743
aton_highway1	0.592
aton_highway3	0.801
aton_room	0.623
aton_campus	0.564
aton_hallway	0.690
aton_lab	0.551

Table 1.2: Datasets and their $\alpha_{\%\Delta}$ correlations to *coneR1**.

Dataset	ρ_{SIFT}
PETS1	-0.057
PETS2	-0.727
aton_highway1	0.009
aton_highway3	0.350
aton_room	-0.079
aton_campus	0.218
aton_hallway	-0.201
aton_lab	0.046

Table 1.3: Datasets and their $SIFT$ correlations to *coneR1**. Non-insignificant correlations are observed, but are inconsistent.

correlation between the two sets implies that both α_{dB} and $\alpha_{\%\Delta}$ will provide a *coneR1′* that will improve shadow removal across the selected datasets.

PETS1 is the primary outlier with a correlation coefficient of approximately 19% for both attenuation models. While both PETS2 and PETS1 experience illumination change within the extracted samples, PETS2 and *coneR1** have a correlation coefficient of approximately 74%. During the illumination change in PETS2, in which the average brightness of the entire

scene decreases by 23%, observed attenuation proportionally decreases by 28%. We observe *coneR1** decreases by 37%. PETS1 experiences a similar illumination change (21%), and an attenuation change of 32%, but no significant corresponding fluctuation in *coneR1**. Illumination and parametric fluctuation was obtained by measuring these values at the beginning and end of the illumination change within the dataset, a range of 22 frames for PETS2, and 45 frames for PETS1. One possible explanation for this discrepancy is that because every pixel is darkened by roughly the same amount due to the illumination shift, the attenuation changes, while the normalized value *coneR1** does not. However, since this behavior is not evident in PETS2 as well, there are likely undiscovered factors influencing PETS1's poor correlation coefficient.

Both α_{dB} and $\alpha_{\%\Delta}$ are illustrated in Figure **??** to contrast the trends of each attenuation model.

The results in Tables **??** and **??** indicate that some datasets benefit from the α_{dB} model, while others benefit from the $\alpha_{\%\Delta}$ model. While the correlation found using the two models are comparable, we use the $\alpha_{\%\Delta}$ model in Eqn. **??**, when calculating the substitute parameter *coneR1′*. This is because the $\alpha_{\%\Delta}$ model provides a closer fit to *coneR1**, in terms of the magnitude shift required (covered in detail in section **??**. An example of this closer fit is found in the qualitative comparison Figure **??**(a).

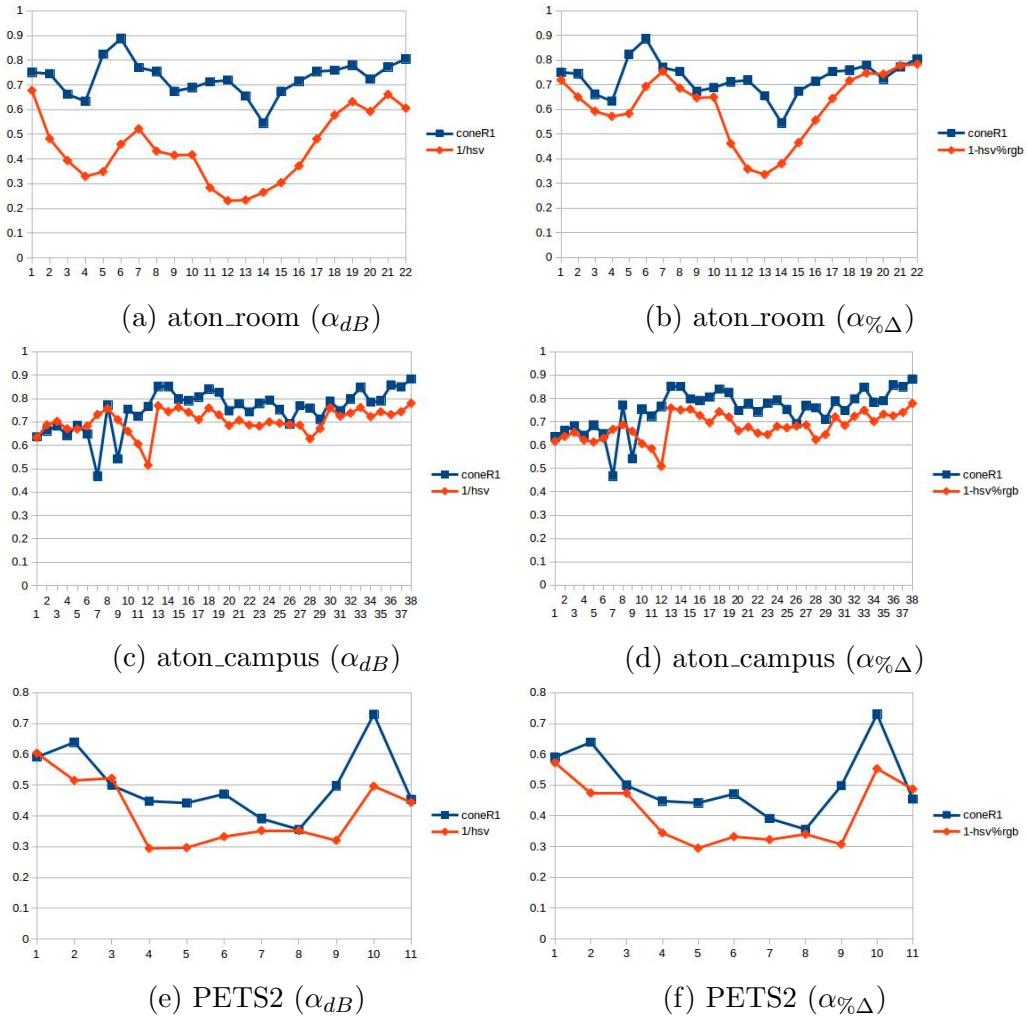

(a) aton_room (α_{dB})

(b) aton_room ($\alpha_{\%\Delta}$)

(c) aton_campus (α_{dB})

(d) aton_campus ($\alpha_{\%\Delta}$)

(e) PETS2 (α_{dB})

(f) PETS2 ($\alpha_{\%\Delta}$)

Figure 1.3: Qualitative comparison of α_{dB} (left) and $\alpha_{\%\Delta}$ (right) across datasets. (Full results for each dataset is found in the appendix)

1.1.2 Correlation Improvements

In sections **??** and **??**, we detail indirect environmental properties that may be used to improve correlation. We conduct sensitivity analysis on the two properties, based on low-contrast SIFT keypoints and brightness models.

Low-contrast SIFT keypoints are analyzed within a frame and are used to produce a scaling factor that is applied to observed attenuation $\alpha_{\%\Delta}$. From this analysis we determine that the low-contrast scaling factor provides boosts to correlation in select datasets, while proving detrimental to others.

We demonstrate that correlation (both ρ_{dB} and $\rho_{\%\Delta}$) are sensitive to varying brightness models, by contrasting their effects across datasets. We show quantifiable and predictable effects on the α_{dB} attenuation model, indicating that outdoor datasets consistently prefer to use the HSP and Luma brightness models, while indoor datasets are not sensitive to varying brightness models. Similar analysis is performed regarding $\rho_{\%\Delta}$; however, differences intrinsic to attenuation calculation prevent similar predictions from being made.

Low-contrast SIFT Keypoints

Using Eqn. **??** defined in section **??**, $SIFT_{fg/bg}$ is calculated per frame and multiplied against the observed average attenuation. $SIFT_{\%C}(f)$ represents the ratio of total low contrast SIFT features to normal SIFT features within a frame f.

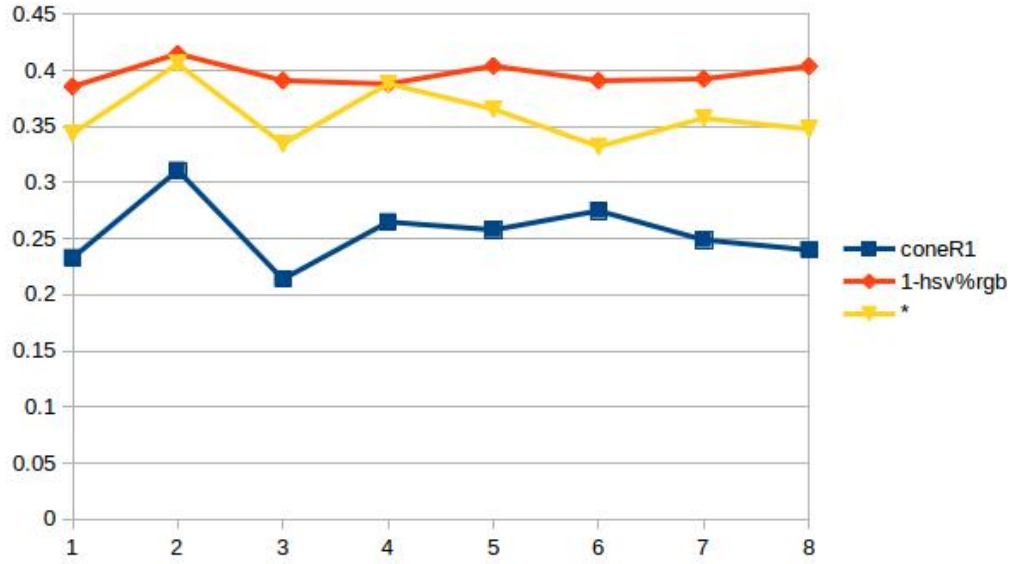

Figure 1.4: $SIFT_{fg/bg}$ multiplication's effect on correlation for the dataset aton_highway1. The observed attenuation $\alpha_{\%\Delta}$ (orange), is multiplied by the calculated $SIFT_{fg/bg}$ on a per frame basis. The resultant, shown in yellow, represents a closer fit to *coneR1** (blue).

$$SIFT_{fg/bg} = \frac{SIFT_{\%C}(fg)}{SIFT_{\%C}(bg)} \tag{1.2}$$

Figure **??** shows the multiplication's effect on the aton_highway1 dataset. Figure **??** and Table **??** detail the effects on correlation ($\rho_{\%\Delta}$) for each dataset.

Table **??** shows that modulating $\alpha_{\%\Delta}$ by $SIFT_{fg/bg}$ produces inconsistent results. For aton_highway1, aton_room, and aton_campus, the operation produced favorable results. However, for all other datasets it produced unfavorable or negligible results. The datasets that had the greatest improvements, aton_highway1 and aton_campus, contain the darkest shadows. Simi-

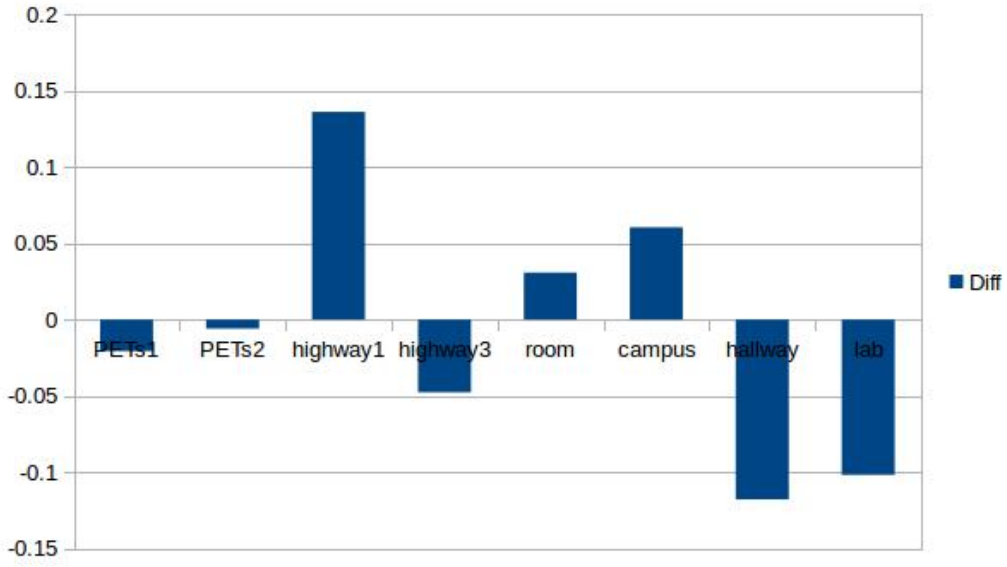

Figure 1.5: Visualization of correlation shifts ($\rho_{\%\Delta}$) found in Table **??**.

Dataset	$\rho_{\%\Delta}$ Shift (%)
PETS1	-2.06
PETS2	-0.58
aton_highway1	+13.62
aton_highway3	-4.76
aton_room	+3.087
aton_campus	+6.06
aton_hallway	-11.78
aton_lab	-10.17

Table 1.4: Correlation shifts ($\rho_{\%\Delta}$) when $SIFT_{fg/bg}$ is multiplied against observed attenuation $\alpha_{\%\Delta}$.

larly, the most negatively affected datasets, aton_hallway and aton_lab, have the faintest shadows. From this observation, we posit that there is a range of shadow brightness in which the saturation channel is affected enough (detailed in section **??**) to be detectable as a low-contrast SIFT keypoint, and therefore that range benefits from analyzing low-contrast SIFT keypoints. This validates the assumption that low-contrast SIFT features, while not in direct correlation with *coneR1**, can provide indirect benefits by improving the existing correlation ($\rho_{\%\Delta}$) depending on the environment. Future work using low-contrast SIFT keypoints begins with determining this threshold.

Brightness Models - ρ_{dB} Attenuation Model

In addition to differing responses to attenuation models, datasets also respond uniquely to varying brightness models. Figure **??** illustrates how differing brightness models affects the correlation coefficient of attenuation. Table **??** enumerates the correlative changes experienced by each dataset when subjected to a range of brightness models. These results are illustrated in Figure **??**.

Two distinct response trends are observed in Figure **??**. These trends are shown in Figure **??**: outdoor datasets (PETS1, PETS2, aton_highway3, and aton_campus) share a similar response to the various brightness models, while indoor datasets (aton_room, aton_hallway, and aton_lab) also share a similar response. Table **??** indicates that ρ_{dB} is sensitive to change in brightness models amongst outdoor datasets (Figure **??**(a)), with HSP and Luma

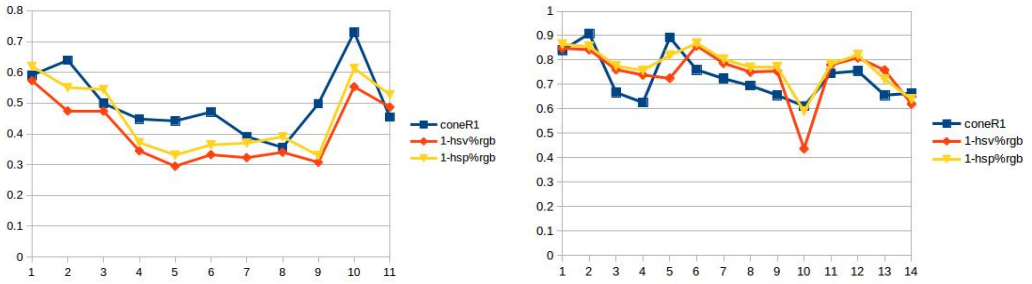

(a) PETS2 (b) aton_lab

Figure 1.6: Example contrasting correlation improvements of the HSP model (yellow) against HSV (red) and *coneR1** (blue).

Dataset	**HSV** ρ_{dB}	**HSP** ρ_{dB}	**HSI** ρ_{dB}	**HSL** ρ_{dB}	**Y'** ρ_{dB}	**Norm** ρ_{dB}
PETS1	0.199	0.227	0.202	0.190	0.222	0.205
PETS2	0.671	0.710	0.690	0.653	0.696	0.695
aton_highway1	0.684	0.477	0.524	0.560	0.471	0.669
aton_highway3	0.742	0.814	0.795	0.780	0.816	0.773
aton_campus	0.359	0.483	0.430	0.416	0.487	0.420
aton_room	0.548	0.528	0.532	0.536	0.527	0.532
aton_hallway	0.656	0.625	0.617	0.622	0.618	0.601
aton_lab	0.695	0.710	0.705	0.717	0.710	0.708

Table 1.5: Datasets and their correlations to *coneR1** (α_{dB}) against Brightness models. Outdoor (top) and Indoor (bottom) scenes are grouped appropriately.

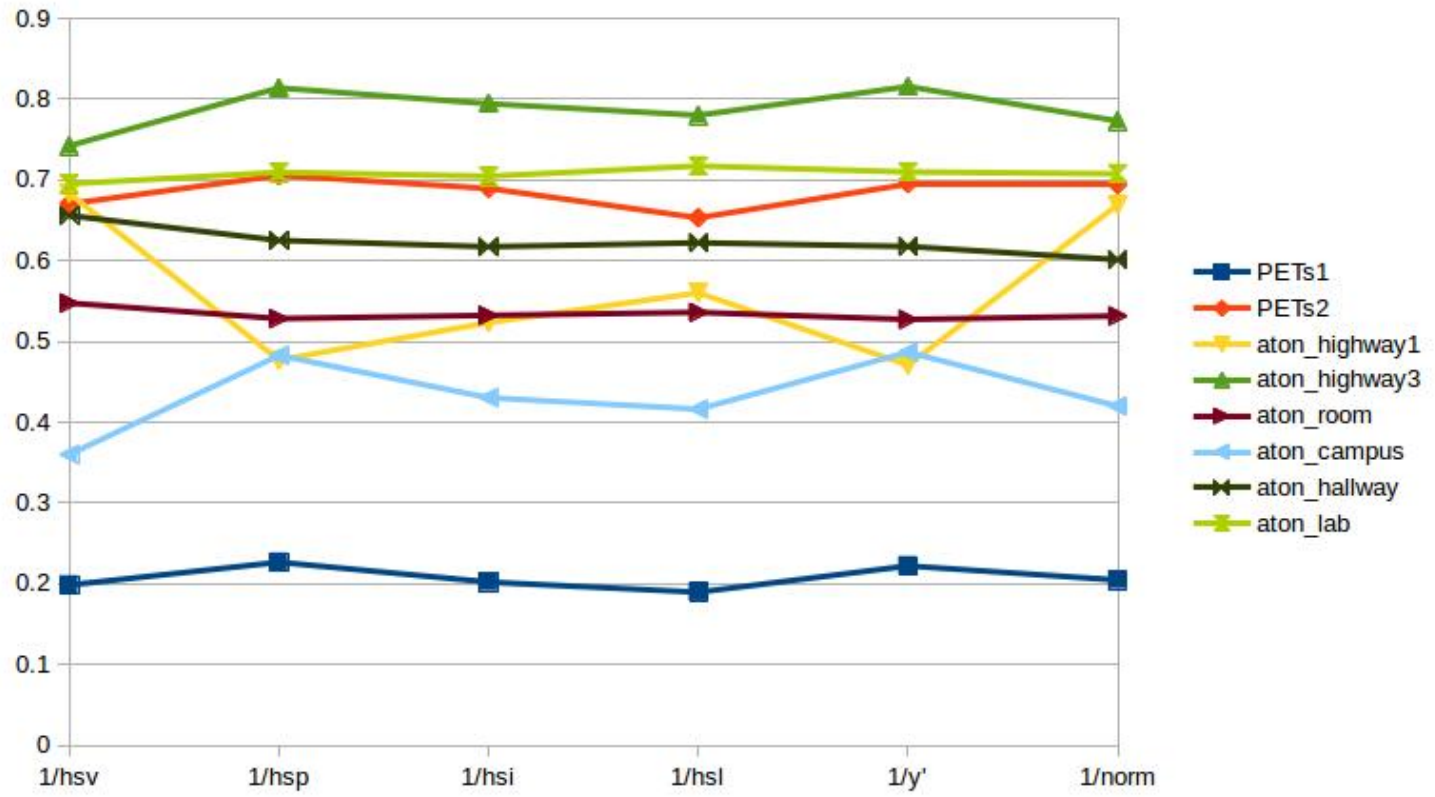

Figure 1.7: Datasets and their correlations (y-axis)to *coneR1** (α_{dB}) against Brightness models (x-axis).

(Y') consistently providing the highest correlations. Indoor datasets (Figure **??**(b)) exhibit negligible sensitivity to brightness model change for ρ_{dB} attenuation. From this indication, we deduce that utilizing either the HSP or Luma brightness model improves correlation (ρ_{dB}) for outdoor scenes.

Furthermore, we can predict when to utilize the HSP/Luma models for better (dB) correlation, by measuring the *red-green color bias* (defined below) corresponding to shadow regions in a dataset. The difference in brightness models can be primarily characterized by their individual treatments of color content in a pixel, i.e., both Y' and HSP weight the channels of an RGB image by scaling factors relevant to human perception, while HSV simply takes the largest color channel value as the brightness. We differentiate between the datasets by measuring the average red-green color bias (β_p^{RG}, for pixel p) present in shadow pixels. To determine color bias, we use the color shift (ΔRGB) from a foreground shadow pixel to an illuminated background pixel. We define the red-green color bias as the observed blue color shift of a foreground shadow pixel p subtracted from the mean of observed red and green color shifts (Eqn. **??**).

$$\beta_p^{RG} = \frac{\Delta R_p + \Delta G_p}{2} - \Delta B_p \tag{1.3}$$

This operation is performed on each foreground pixel that is darker than its corresponding background pixel, and averaged into β_{RG}^f, the average red-green color bias per frame. The values of β^{RG} are contingent on the repre-

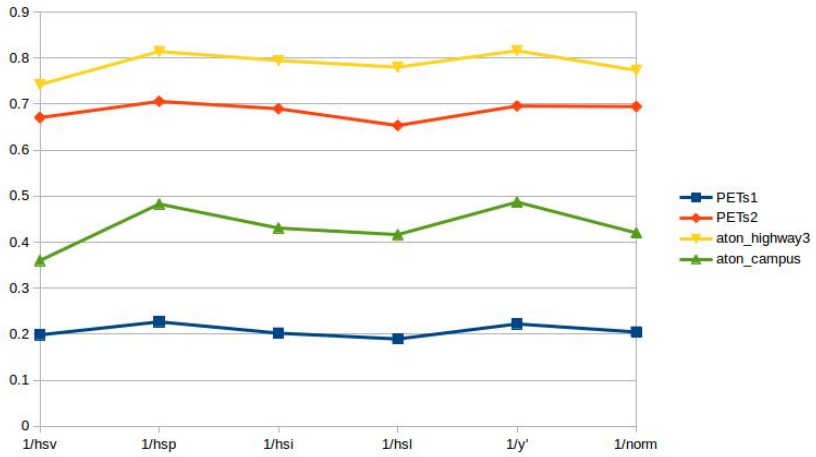

(a)

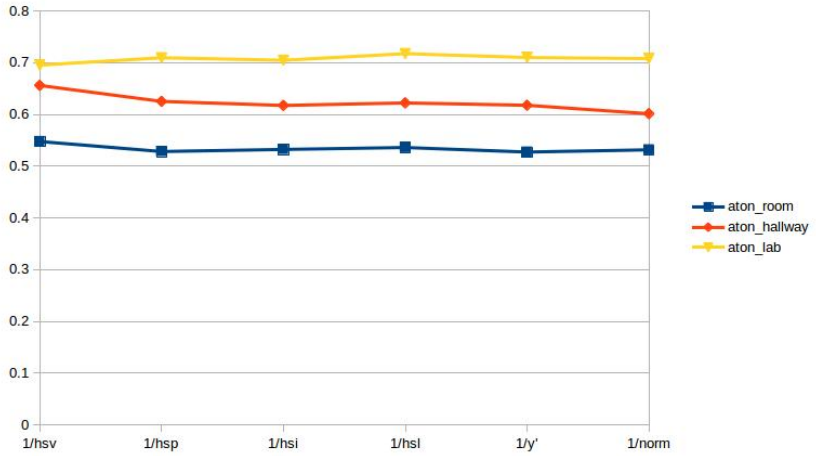

(b)

Figure 1.8: Outdoor datasets (a) share a common response to varying brightness models. In contrast, indoor datasets (b) share a insensitivity to varying brightness models.

Dataset	β^{RG}
PETS1	15.03
PETS2	7.57
aton_highway1	6.69
aton_highway3	2.56
aton_campus	3.32
aton_room	1.64
aton_hallway	-0.26
aton_lab	0.35

Table 1.6: Red-green bias for each dataset. β^{RG} represents the average of the β_f^{RG} for each frame in a dataset. Outdoor (top) and Indoor (bottom) scenes are grouped appropriately.

sentation of the RGB channels in an image. In our study, each channel has a range of $(0, 255)$. As seen in Table **??**, outdoor datasets display consistently higher β^{RG} values.

The exception to this grouping of outdoor and indoor datasets is aton_highway1, an outdoor dastaset that has a response reciprocal to that of most outdoor environments. Figure **??** illustrates the mirrored nature of aton_highway1's response. aton_highway1 contains the darkest cast shadows in relation to its background model. The relative low points, HSP and Luma, both attempt to weight brightness according to color information. The applied weights are the only differing factor in the HSP and Norm methods. Therefore, we conclude that the consideration of color shift is a detriment to aton_highway1's ρ_{dB} correlations.

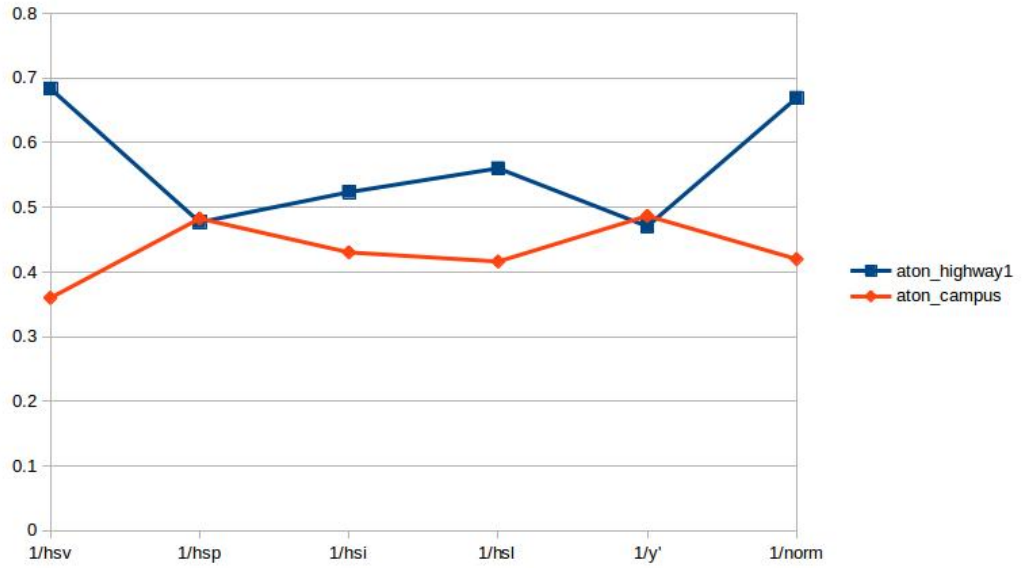

Figure 1.9: aton_highway1's response to various brightness models behaves opposite to other outdoor datasets.

Brightness Models - $\rho_{\%\Delta}$ Attenuation Model

Results indicating correlations ($\rho_{\%\Delta}$) per brightness model are enumerated in Table **??**. These results are illustrated in Figure **??**.

It is important to note that Figure **??** does not exhibit the trends indicated by the α_{dB} model in Figure **??**. The datasets are separated into outdoor/indoor datasets in Figure **??**. Some datasets, such as PETS1, PETS2, aton_highway3, and aton_room, demonstrate similar responses to those observed in Figure **??**. However, aton_lab, aton_hallway, and aton_campus behave erratically in comparison to their corresponding α_{dB} responses. The disparity between the two brightness responses can be attributed to the vectorization of the $\alpha_{\%\Delta}$ model, which calculates the brightness of the vector

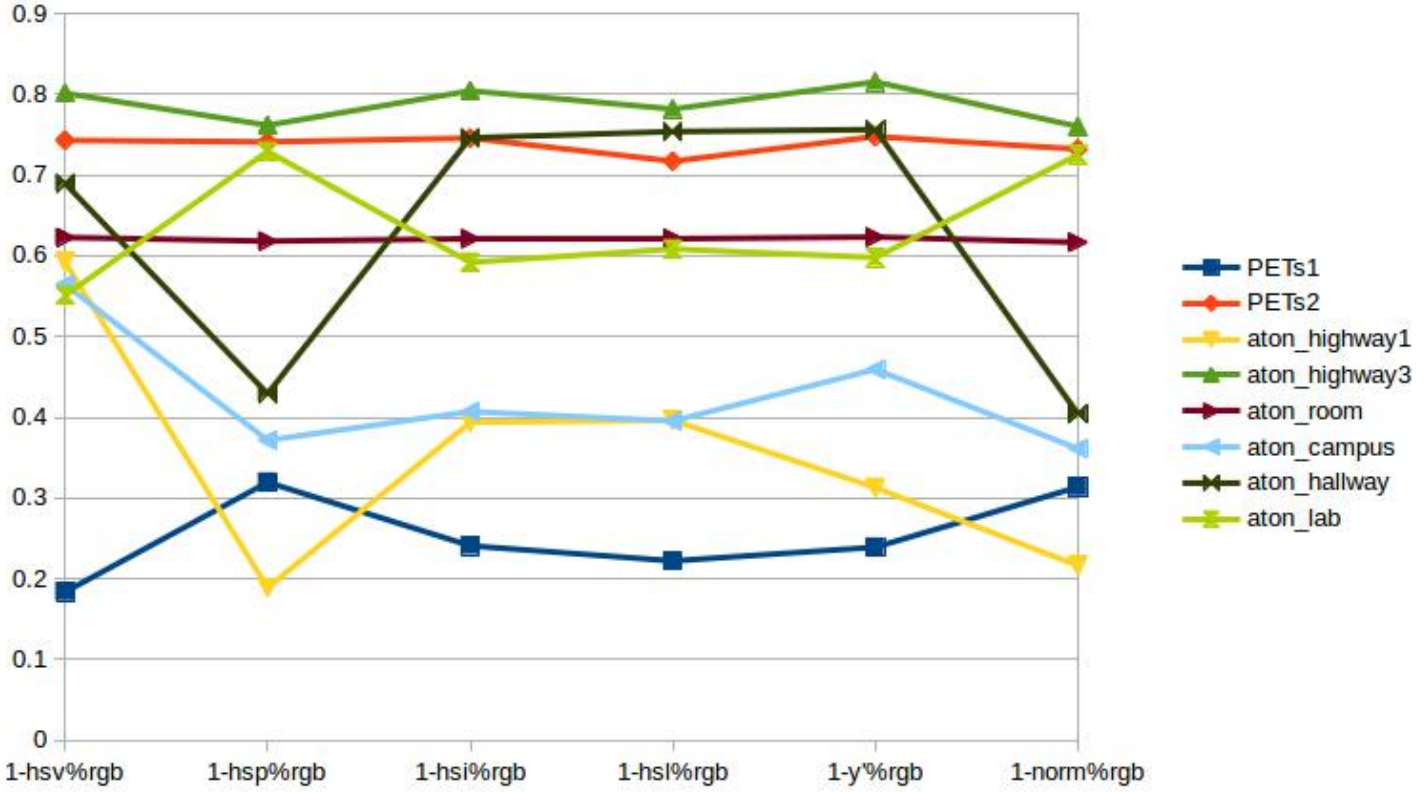

Figure 1.10: Datasets and their correlations (y-axis)to *coneR1** ($\alpha_{\%\Delta}$) against Brightness models (x-axis).

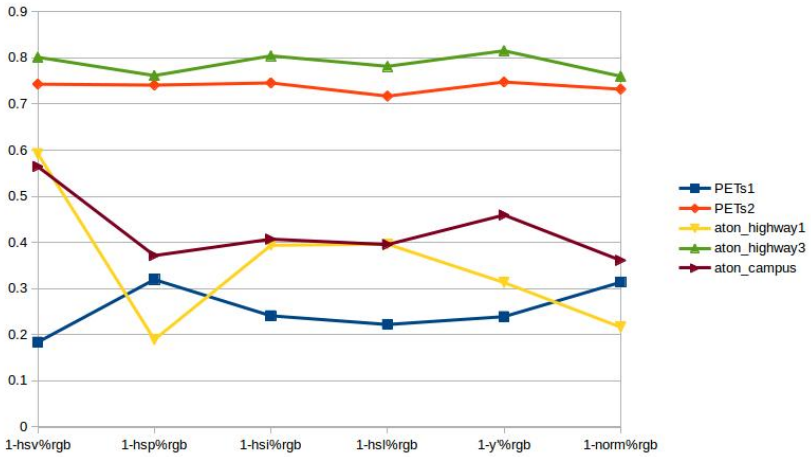

(a)

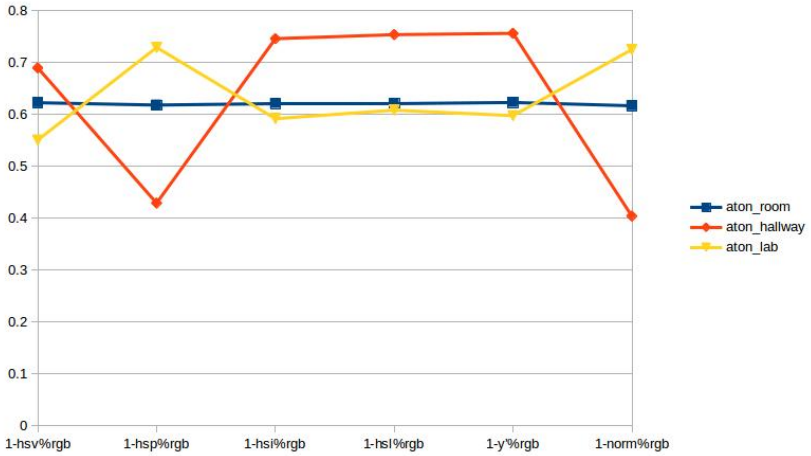

(b)

Figure 1.11: (a) Outdoor datasets. (b) Indoor datasets.

Dataset	HSV $\rho_{\%\Delta}$	HSP $\rho_{\%\Delta}$	HSI $\rho_{\%\Delta}$	HSL $\rho_{\%\Delta}$	Y' $\rho_{\%\Delta}$	Norm $\rho_{\%\Delta}$
PETS1	0.183	0.320	0.241	0.222	0.239	0.314
PETS2	0.743	0.741	0.746	0.717	0.747	0.732
aton_highway1	0.592	0.189	0.393	0.396	0.313	0.216
aton_highway3	0.801	0.761	0.804	0.781	0.815	0.760
aton_campus	0.564	0.371	0.407	0.395	0.459	0.361
aton_room	0.622	0.618	0.621	0.621	0.623	0.616
aton_hallway	0.689	0.429	0.746	0.754	0.756	0.404
aton_lab	0.551	0.729	0.592	0.608	0.597	0.725

Table 1.7: Datasets and their correlations to *coneR1** ($\alpha_{\%\Delta}$) against Brightness models. Outdoor (top) and Indoor (bottom) scenes are grouped appropriately.

between a foreground and background pixel. For example, a pixel p_1 is represented by the RGB values $(25, 50, 75)$, and a second pixel p_2 is $(75, 50, 25)$. Using the HSV brightness model, we calculate the brightness of each pixel to be 75. The α_{dB} model results in 1.0, or no attenuation. The $\alpha_{\%\Delta}$ model calculates the brightness change of the difference, $p_2 - p_1 = (50, 0, -50)$. Using the HSV model, $\alpha_{\%\Delta}$ reports a brightness shift of 50 units, with a resulting attenuation of $50/75 = 0.66$. We conclude the attenuation model $\alpha_{\%\Delta}$ is not predictably sensitive to a change in brightness model.

1.2 Parameter Model Results

The primary challenge in adapting observed average attenuation into an arbitrary model for shadow removal improvement lies in understanding the necessary translation between observed attenuation and *coneR1**. Utilizing

the formulae specified in section **??**, a coarse-grained model is developed.

Applied to an arbitrary frame, attenuation ($\alpha_{\%\Delta}$) and color magnitude shift (ΔRGB) are analyzed and used to create the necessary translation ($shift_{\alpha}$). This analysis is performed on each brightness model, seen in Figure **??**.

Using ΔRGB, $\alpha_{\%\Delta}$, and $shift_{\alpha}$, we calculate the adapted variable $coneR1'$. Illustrated results of this model are displayed in Figure **??** for the datasets aton_highway1 and aton_highway3. The resultant of the model ($coneR1'$), shown in **orange**, retains correlative properties observed prior while providing a reasonable estimate for required translation.

1.2.1 Analysis

Figure **??** illustrates the resulting detection and discrimination rates of shadow removal using the adapted parameter $coneR1'$, contrasting the generated results (orange) with detection/discrimination determined via the original naive method (blue). Detection and discrimination are averaged per frame for each dataset. Quantitative results are shown in Tables **??** and **??**.

Results indicate that for a majority of datasets, small amounts of shadow detection accuracy is sacrificed for disproportionate increases in shadow discrimination. Figure **??** qualitatively illustrates shadow removal improvements using the adaptive method for datasets aton_campus and aton_room.

aton_highway1 proved anomalous, trading in nearly equal part detection for discrimination, arriving at a net modest positive of 1.2%. We theorize

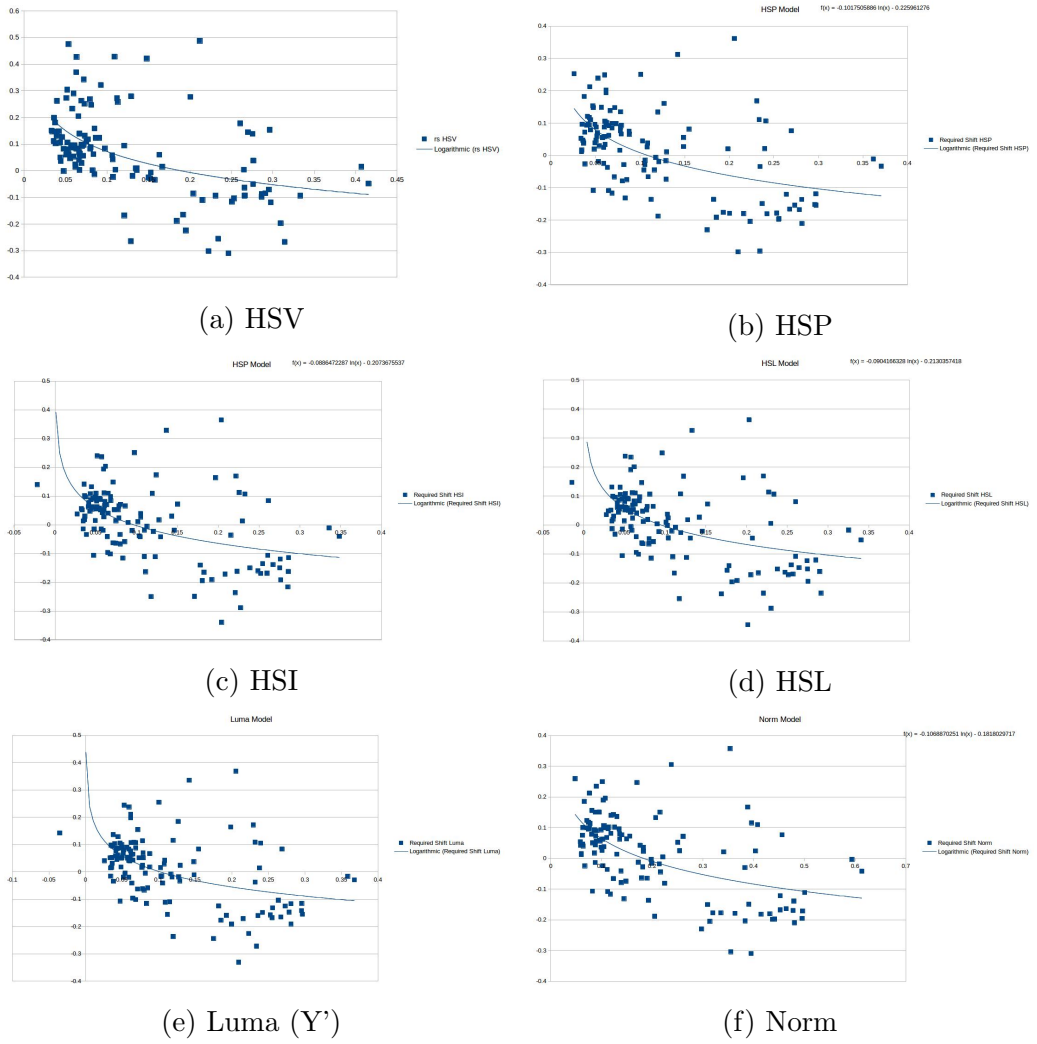

(a) HSV (b) HSP

(c) HSI (d) HSL

(e) Luma (Y') (f) Norm

Figure 1.12: For each brightness model, ΔRGB is plotted against $shift_{req.}$. The general model for each brightness calculation is formed through a best-fit logarithm.

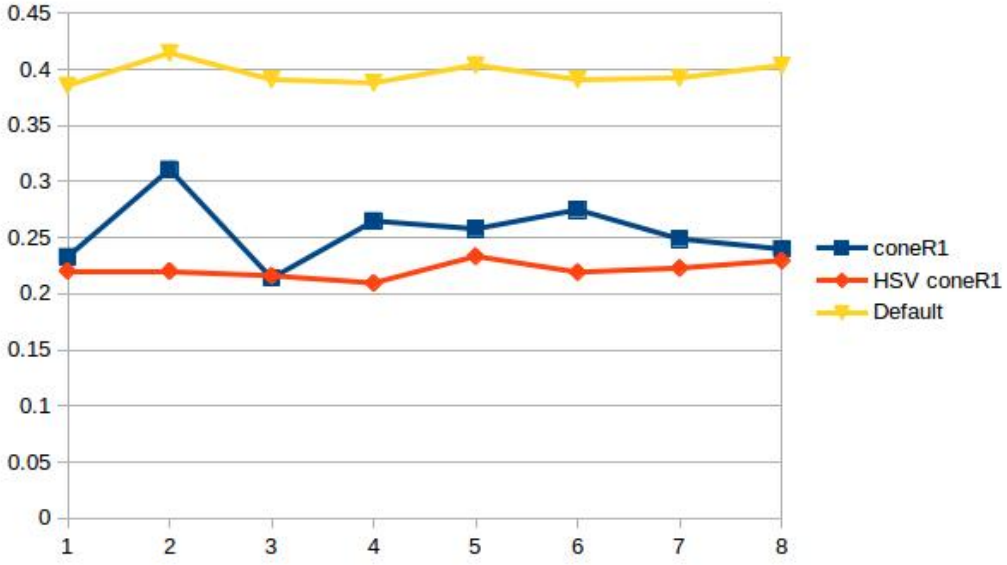

(a) aton_highway1

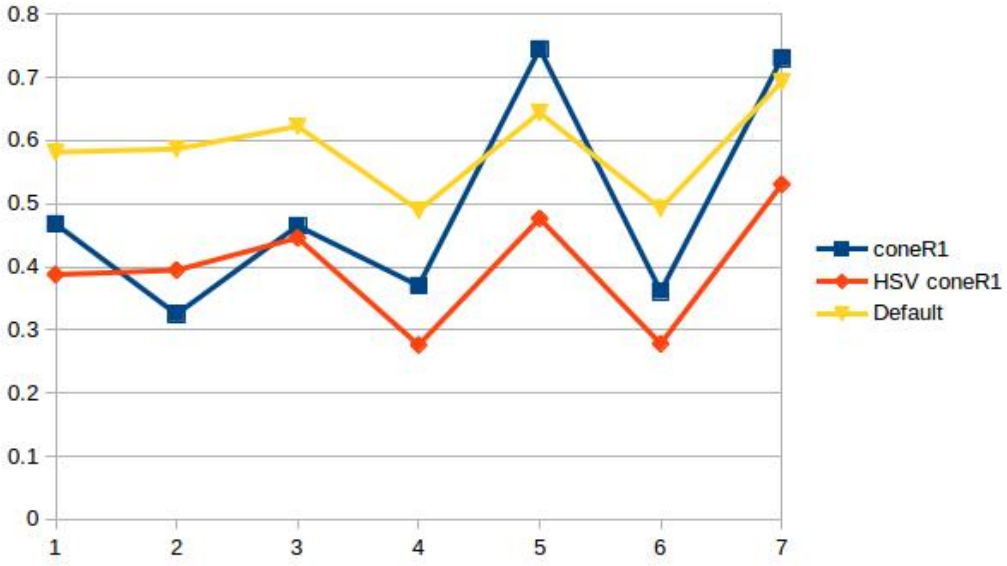

(b) aton_highway3

Figure 1.13: Adaptively tuned *coneR1′* parameter (orange) charted against *coneR1** (blue) and average attenuation ($\alpha_{\%\Delta}$) (yellow). All results can be found in the appendix.

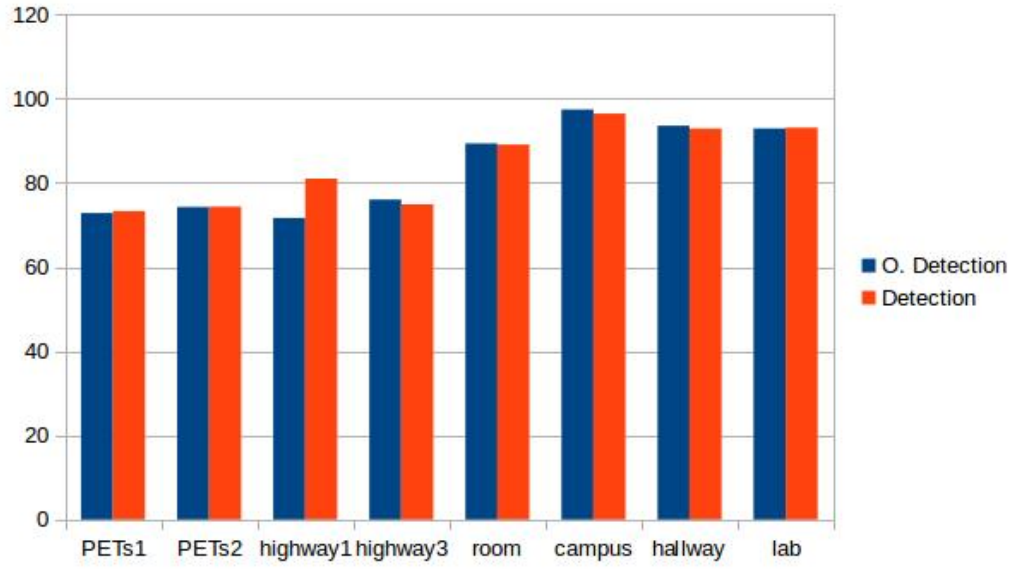

(a)

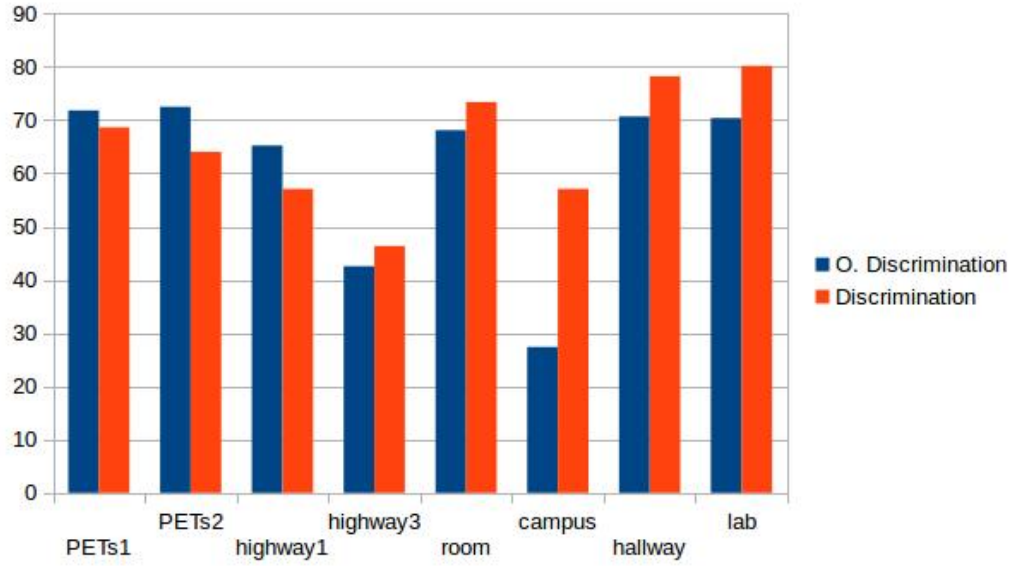

(b)

Figure 1.14: Average detection (a) and average discrimination (b) calculated using the HSV parameter model, for each dataset.

Dataset	η (%)	+/- (%)
PETS1	73.28	+0.459
PETS2	74.34	+0.056
aton_highway1	80.99	+9.353
aton_highway3	74.88	-1.154
aton_room	89.10	-0.264
aton_campus	96.46	-0.976
aton_hallway	92.91	-0.660
aton_lab	93.12	+0.192

Table 1.8: Average detection (η) calculated from the adapted *coneR1′* (left). η is compared against original naive detection (*coneR1*= 0.3). The difference (right) is represented as a percentage.

Dataset	ξ (%)	+/- (%)
PETS1	68.61	-3.176
PETS2	64.04	-8.458
aton_highway1	57.05	-8.172
aton_highway3	46.35	+3.802
aton_room	73.36	+5.278
aton_campus	57.05	+29.67
aton_hallway	78.22	+7.549
aton_lab	80.16	+9.787

Table 1.9: Average discrimination (ξ) calculated from the adapted *coneR1′* (left). ξ is compared against original naive discrimination (*coneR1*= 0.3). The difference (right) is represented as a percentage.

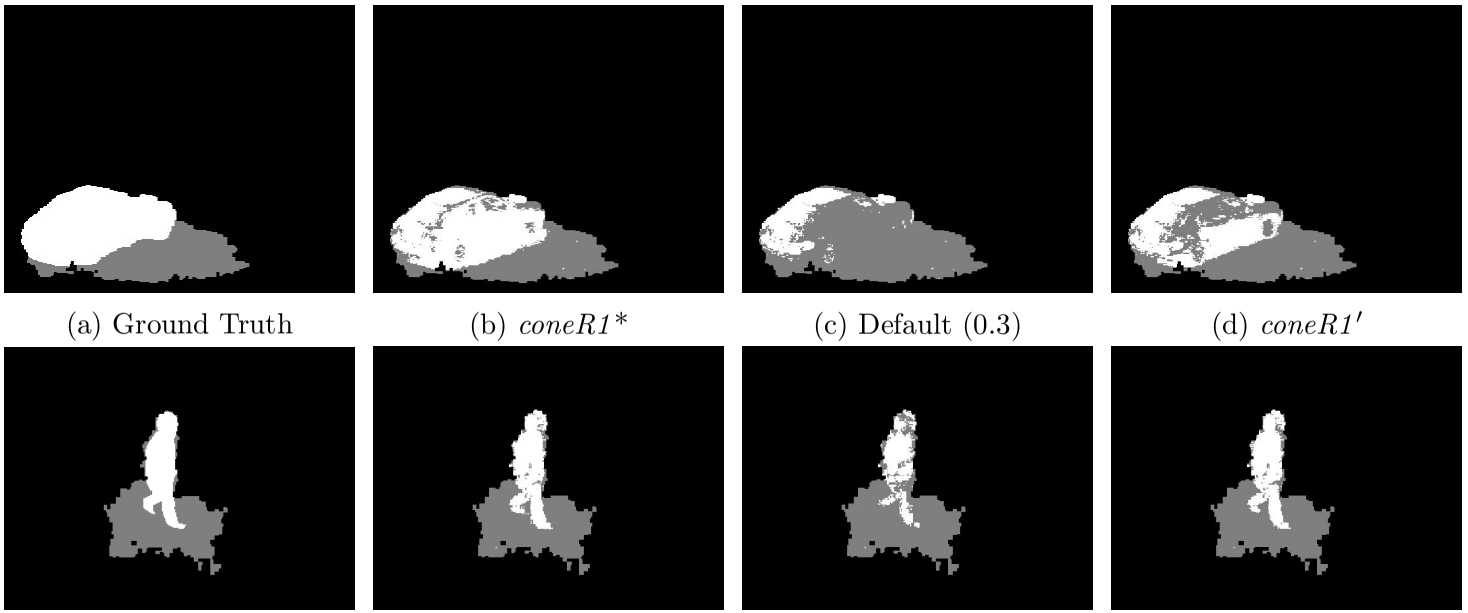

(a) Ground Truth (b) *coneR1** (c) Default (0.3) (d) *coneR1′*

(e) Ground Truth (f) *coneR1** (g) Default (0.3) (h) *coneR1′*

Figure 1.15: Qualitative shadow removal improvement. (a - d) feature the aton_campus dataset, and (e - h) feature the aton_room datasets.

aton_highway1's inconsistent behavior is due to it possessing the darkest cast shadows. Furthermore, aton_highway1 attenuates non-linearly (as expected of an outdoor scene), yet by visual inspection, is desaturated. The combination of the strong shadows and the low saturation of the frame allows a larger population of candidate shadows pixels to be gathered. Due to these conditions, foreground *object* pixels are more likely to appear identical to shadow pixels, in both color information and relative distance from its background pixel. The confluence of these scene characteristics renders aton_highway1 less predictable than other datasets.

PETS1 and PETS2 also do not conform to the upward trends seen in the majority of datasets. In the case of PETS1, the low correlation coefficient infers the poor detection/discrimination observed. More interestingly, PETS2 experiences the same degradation of performance as PETS1, but has a much stronger correlation coefficient, seen in Table **??**. This decoupling of correlation and accuracy stems from the generalized model of improvement translating the observed average attenuation necessarily. This is illustrated in Figure **??**. The model overcompensates for observed color shift (ΔRGB) in PETS2, due to the illumination change in the dataset. The misrepresentation of attenuation (and thereby ΔRGB) of cast shadows in PETS2 results in the unnecessary 'downward' translation, impacting PETS2's shadow discrimination accuracy.

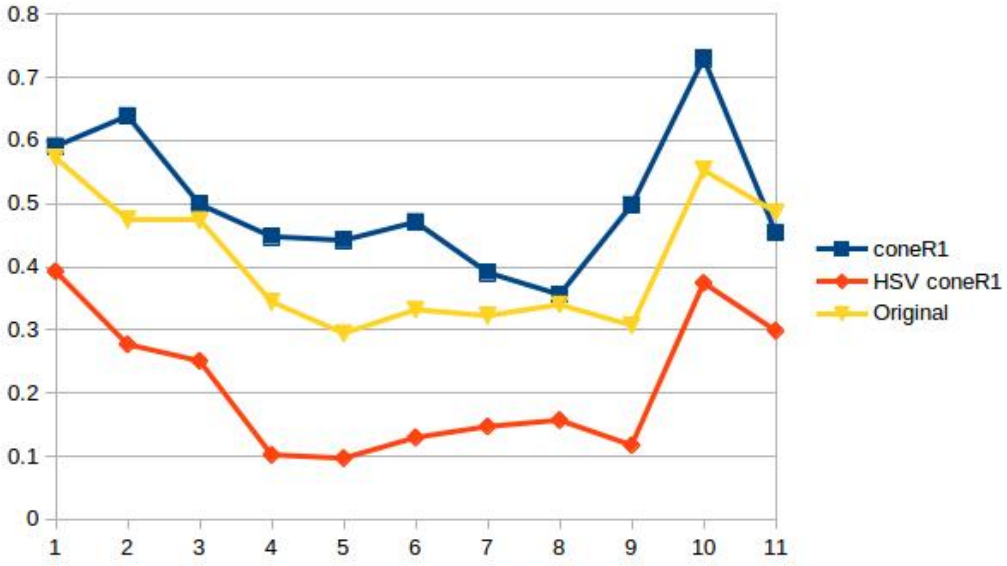

Figure 1.16: For PETS2, the adapted parameter *coneR1′* (orange) is erroneously shifted downwards. The originally observed attenuation ($\alpha_{\%\Delta}$) is shown in yellow.

1.2.2 Brightness Models and Shadow Removal

It is noted in section **??** that the correlative changes observed in varying brightness models are not consistent from the α_{dB} to the $\alpha_{\%\Delta}$ model of attenuation. While correlation coefficient and shadow removal improvement are often related, it is entirely possible to observe cases in which the opposite is true. For example, two vectors are perfectly correlated, $a^T = [20, 10]$ and $b^T = [10, 0]$. By increasing b^T to [10, 10], the vectors' correlation coefficient is greatly reduced, while their overall fit has been improved. The following results demonstrate this concept, uncoupling the correlation changes recorded in section **??** from shadow removal improvement. Figure **??** illustrates detec-

tion (blue) and discrimination (orange) rates within a dataset across varying brightness model, using the $\alpha_{\%\Delta}$ attenuation model.

The effect of varying brightness models on shadow removal improvement adheres to correlation trends, identified in section **??**, for the datasets aton_room, aton_campus, aton_hallway, and aton_lab. For these datasets, shadow detection accuracy is improved up to 2%, and shadow discrimination is improved up to 3%. For the remaining datasets, varying the brightness model imparted change on only the correlation, and did not affect detection or discrimination. These results indicate that while correlation ($\rho_{\%\Delta}$) is sensitive to brightness model change, the resulting shadow removal itself is not consistently sensitive to correlation changes. Furthermore, the datasets that are sensitive to change in brightness model are only affected marginally, in contrast to the correlation responses in section **??**.

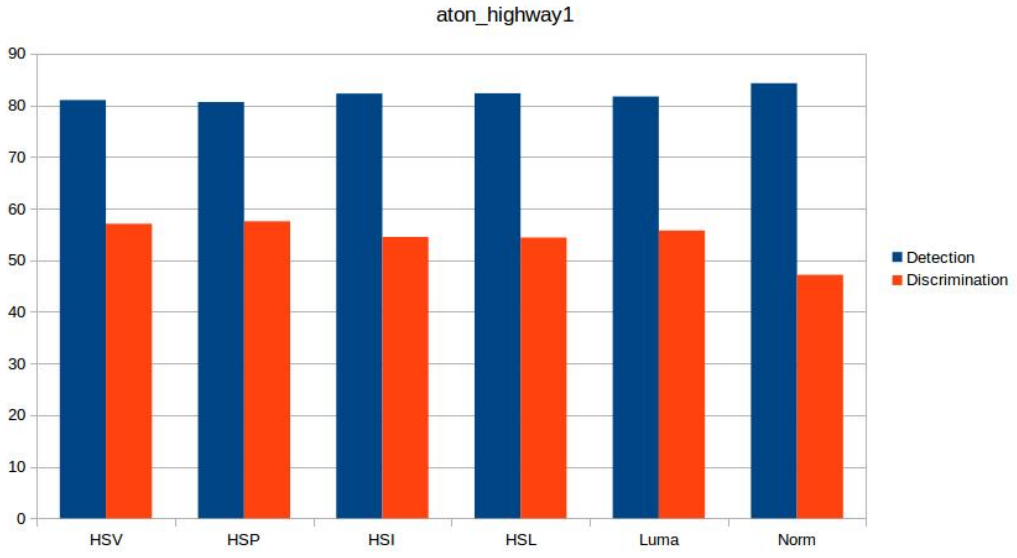

(a) aton_highway1

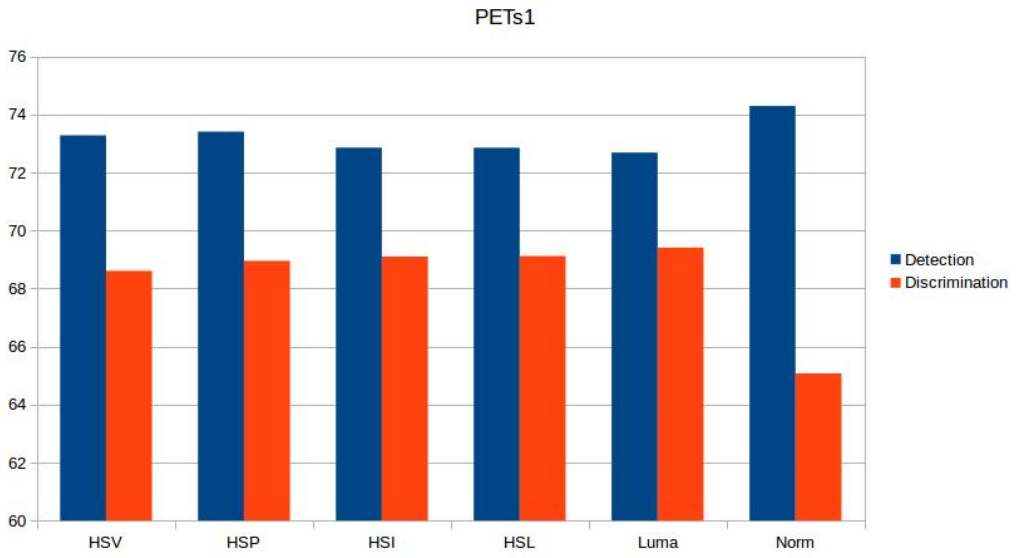

(b) PETS1

Figure 1.17: Detection (blue) and Discrimination (orange) for each brightness model. Full results for all datasets can be found in the appendix.